Spin wave mode coupling in antiskyrmions induced by rotational symmetry breaking

Zhen Cheng [1], Haoran Chen,[1] Siying Huang,[1] and Yizheng Wu [1,2,3,*]

[1]*Department of Physics and State Key Laboratory of Surface Physics, Fudan University, Shanghai 200433, China*
[2]*Shanghai Research Center for Quantum Sciences, Shanghai 201315, China*
[3]*Shanghai Key Laboratory of Metasurfaces for Light Manipulation, Fudan University, Shanghai 200433, China*

The antiskyrmion, as a topological structure, can be stabilized by anisotropic Dzyaloshinskii-Moriya interaction. We investigated the dynamic properties of antiskyrmions through micromagnetic simulations. The field-dependent evolution of the antiskyrmion expresses a square shape or an elongated shape, due to its spin configuration with the combination of Néel-type and Bloch-type walls. This spin configuration with the broken rotational symmetry leads to a notable mode coupling between the breathing mode and the azimuthal spin wave mode under microwave excitation. The same mode coupling can also exist in the skyrmion system with a small in-plane magnetic anisotropy. Our findings emphasize that the rotational symmetry of the spin configuration may play a significant role in the dynamic properties of antiskyrmions and their relevance to magnonics applications.

I. INTRODUCTION

Topological spin structures have gained significant attention since the prediction and experimental observation of magnetic skyrmions [1–6]. Skyrmions have chiral spin structures and can be stabilized by the Dzyaloshinskii-Moriya interaction (DMI) [7,8], dipolar interaction [9–11], and frustrated exchange interaction [12–14]. As an antisymmetric exchange interaction, DMI exists in systems that lack structural inversion symmetry and favors the perpendicular alignment between neighboring spins. Usually, skyrmions in bulk materials such as MnSi have homochiral Bloch-type magnetization rotation [15], but in thin film systems, they have homochiral Néel-type magnetization rotation due to the interfacial DMI [16–19]. Studies on the generation, manipulation, and detection of skyrmions have triggered many interesting skyrmion-based applications such as racetrack memory [20,21], nano-oscillator [22,23], and neuromorphic computing [24–26].

Due to the opposite topological charge, antiskyrmions and skyrmions can be considered counterparts to each other. Antiskyrmions can be stabilized by the anisotropic DMI that has opposite signs along two orthogonal in-plane directions [27]. The skyrmion configuration shows homochiral Néel or Bloch magnetization rotations [5,28], but the antiskyrmion configuration shows partly Néel and partly Bloch magnetization rotations [29,30]. Bloch rotation does not produce magnetic charges and thus uses less dipolar energy. In skyrmions, the skyrmion Hall effect always exists independently of the current direction, which significantly limits the application of skyrmion-based racetrack memory [31]. However, in antiskyrmions, the skyrmion Hall effect strongly depends on the current direction, and zero Hall angle can be achieved at certain current directions [32]. Antiskyrmions have been experimentally observed in bulk materials due to the anisotropic DMI [33,34], and in magnetic multilayers stabilized by the dipolar interaction [11] utilizing Lorentz transmission electron microscopy, but antiskyrmions stabilized by the anisotropic DMI have not yet been observed in thin film systems. In thin films such as Fe/W(110), the opposite sign of anisotropic DMI needed for stabilizing antiskyrmions has been theoretically predicted [29].

Resonant dynamics is also very important to the understanding and application of topological spin structures. In skyrmions, a microwave field can excite different resonant dynamic modes, such as the gyration mode, breathing mode, and lateral spin wave modes [35,36], which can be further applied to generate the spin wave emission in skyrmions or skyrmion-antiskyrmion pairs [37,38]. Although most relevant studies were conducted theoretically, several experimental works were also performed to measure the dynamics properties of skyrmions [39–45]. On the other hand, due to its shorter history, there has been limited theoretical investigation into the dynamic response of antiskyrmions. Both the breathing mode and gyration motion of antiskyrmions have been found to be analogous to those in skyrmions [46], and microwave fields can be applied to excite a trochoidal motion of antiskyrmions [47]. The most obvious difference between a skyrmion and an antiskyrmion is the different rotational symmetry; thus the nonrotational symmetric nature of antiskyrmions is expected to have a substantial impact on magnetic dynamic modes.

In this study, we investigated the dynamic behavior of antiskyrmions under microwave field excitation using micromagnetic simulation. The breathing modes are almost identical in both skyrmions and antiskyrmions, but an additional dynamic mode was discovered in antiskyrmions, which can be identified as an azimuthal spin wave mode with a wavelength equal to one-quarter of the circumference of the
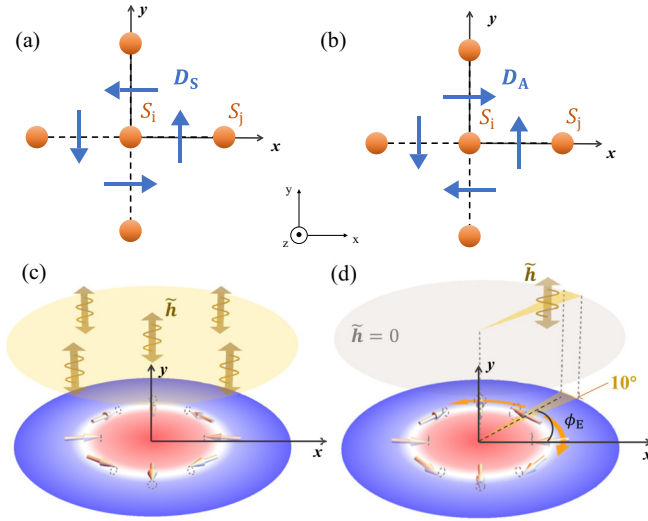
*wuyizheng@fudan.edu.cn

FIG. 1. Schematic diagrams of (a) isotropic and (b) anisotropic DMI. The orange dots represent the atomic spins, and the blue arrows represent the Dzyaloshinskii-Moriya vectors. (c) Schematic illustration of uniform microwave excitation by the uniform ac field $\widetilde{h}_z$ applied uniformly on the structure. (d) Schematic illustration of local microwave excitation with $\widetilde{h}_z$ applied within the area with a $10°$ azimuthal range.

domain wall. By computing the dynamical response under either uniform or nonuniform microwave field excitations, a distinct coupling behavior between the breathing mode and the azimuthal spin wave mode can be observed. By analyzing the effective field distribution within the domain wall of antiskyrmions, we can conclude that the mode coupling can be attributed to the breaking of rotational symmetry in antiskyrmions. The rotational symmetry of magnetization configuration in a skyrmion can be broken by applying a small in-plane magnetic anisotropy, which can induce the additional azimuthal spin wave mode under microwave field excitation. Our results point out that the rotational symmetry of spin configuration may play a significant role in the dynamic properties of antiskyrmions and their related magnonics applications.

This paper is structured as follows: In Sec. II, we present micromagnetic modeling and simulation methods used in this study. Section III unfolds with the initial presentation of the field-dependent evolution of antiskyrmions, followed by an exploration of the dynamic response involving mode coupling through uniform or nonuniform excitation. Additionally, we elucidate the origin of spin wave mode coupling in antiskyrmions arising from rotational symmetry breaking. Section IV succinctly summarizes our key findings.

II. SIMULATION MODEL AND METHODS

We conducted micromagnetic simulations on both skyrmions and antiskyrmions, which can be stabilized by isotropic and anisotropic DMI, respectively. Figures 1(a) and 1(b) show schematic diagrams of isotropic and anisotropic DMI. At the interface between a thin magnetic film and a heavy metal adjacent layer, the Dzyaloshinskii-Moriya vector $\boldsymbol{D}_{ij}$ between spins $\boldsymbol{S}_i$ and $\boldsymbol{S}_j$ on atomic sites i and j usually

lies within the film plane and normal to the distance vector $\boldsymbol{r}_{ij}$. As shown in Fig. 1(a), the $\boldsymbol{D}_{ij}$ vector for isotropic DMI is always parallel or antiparallel to $\boldsymbol{z} \times \boldsymbol{r}_{ij}$, where $\boldsymbol{z}$ represents the normal direction. Thus a skyrmion has homochiral Néel magnetization rotation with rotation symmetry [32]. If the system contains anisotropic DMI with the opposite sign of $\boldsymbol{D}_{ij}$ vectors along the x and y directions, shown in Fig. 1(b), antiskyrmions can emerge. The spin configuration in the domain wall of an antiskyrmion exhibits Néel-type rotation along the x or y axis with opposite chirality, but has Bloch-type rotations at $45°$ away from the x or y axis, as shown in Fig. 1(c). Thus the spin configuration inside the DW of the antiskyrmion shows twofold symmetry. In this study, all the $\boldsymbol{D}_{ij}$ vectors between two neighboring spins have the same magnitude D, which can be varied in the simulation.

The dynamical properties of antiskyrmions and skyrmions were investigated through micromagnetic simulation based on the Landau-Lifshitz equation using MUMAX3 software [48]. MUMAX3 calculates the time derivation of $\boldsymbol{m}$ based on the LLG equation [49] of motion for magnetization dynamics,

$$\frac{\partial \boldsymbol{m}}{\partial t} = -\gamma \boldsymbol{m} \times \boldsymbol{H}_{\mathrm{eff}} + \alpha \boldsymbol{m} \times \frac{\partial \boldsymbol{m}}{\partial t}, \quad (1)$$

where γ is the gyromagnetic ratio, α is the damping constant, and $\boldsymbol{m}$ is the unit magnetization. $\boldsymbol{H}_{\mathrm{eff}}$ is the effective field, and can be calculated with $\boldsymbol{H}_{\mathrm{eff}} = -\frac{1}{\mu_0 M_s} \frac{\partial E}{\partial \boldsymbol{m}}$, where M_s is the saturation magnetization, and E is the total energy density of the system, including the Heisenberg exchange interaction energy $\varepsilon_{\mathrm{ex}}$, the magnetic dipole interaction energy ε_d, magnetic anisotropy energy $\varepsilon_{\mathrm{anis}}$, interfacial DMI energy $\varepsilon_{\mathrm{DMI}}$, and Zeeman energy $\varepsilon_{\mathrm{ext}}$. For the system with perpendicular uniaxial anisotropy, the anisotropy energy can be expressed as $\varepsilon_{\mathrm{anis}} = -K_u (\boldsymbol{m} \cdot \boldsymbol{z})^2$, where K_u is the magnetic anisotropy constant. Furthermore, for DMI energy within a continuous magnetization model [50], it can be expressed as $\varepsilon_{\mathrm{DM}} = D(m_z \frac{\partial m_x}{\partial x} - m_x \frac{\partial m_z}{\partial x}) + D(m_z \frac{\partial m_y}{\partial y} - m_y \frac{\partial m_z}{\partial y})$ for skyrmions, and $\varepsilon_{\mathrm{DM}} = D(m_z \frac{\partial m_x}{\partial x} - m_x \frac{\partial m_z}{\partial x}) - D(m_z \frac{\partial m_y}{\partial y} - m_y \frac{\partial m_z}{\partial y})$ for antiskyrmions. Here, m_x, m_y, and m_z are the components of the unit magnetization, and D is the area unit energy density of DMI.

The simulation was performed mainly on a magnetic disk with a 100 nm diameter and 1 nm thickness, and the unit cell in the simulation is $1 \times 1 \times 1$ nm^3. We used the exchange constant $A = 15$ pJ m^{-1}, perpendicular anisotropy constant $K_u = 1$ MJ m^{-3}, and saturation magnetization $M_s = 1$ MA m^{-1}, similar to the parameters used in Ref. [51]. These parameters are corresponding to a model thin ferromagnetic film with perpendicular anisotropy. For comparison, we also performed studies on square disks with 100 nm length and circular disks with different diameters, and the results yielded similar findings [52].

We first simulated the field-dependent evolution of an antiskyrmion with different DMI strength D. For the system with a fixed D, the magnetization at the core center is initially set along the $+z$ direction, and the rest of the magnetization is set along the $-z$ direction. Then the magnetic structure of the antiskyrmion was relaxed at zero field and further simulated by gradually increasing or decreasing the field H_z. In order to make the system quickly relax into the equilibrium

state, a large damping constant $\alpha = 0.5$ was used. The time-dependent variation of the magnetization during the relaxation process was monitored to ensure that the micromagnetic state converges to the equilibrium state.

The magnetization dynamics of antiskyrmions was further calculated starting from the equilibrium state with different H_z. The excitation modes of the skyrmion are determined from the transient response of the system to a time-varying perpendicular field $\widetilde{h}_z(t)$. A sinc-type field $\widetilde{h}_z(t) = \mu_0 h_0 \mathrm{sinc}(2\pi f_c t)$ with a cutoff frequency of $f_c = 50$ GHz is used to excite the magnetization dynamics. The Fourier transform of the sinc function is a rectangular function; thus the sinc-type field can excite the magnetization dynamics up to 50 GHz. A lower damping constant α of 0.01 was used in the simulation of the dynamical properties. The transient dynamics was computed over 20 ns, with the data recorded every 5 ps. During the dynamics excitation, the dynamical magnetization $\widetilde{m}_z(t)$ at each unit cell was saved, and the power spectral density (PSD) $s(f)$ from each $\widetilde{m}_z(t)$ was calculated using a fast Fourier transform (FFT) algorithm. Thus the spatial distributions of both the magnitude and phase of each excitation mode can be obtained. We also summarized all the amplitudes of $s(f)$ from each unit cell, i.e., $S(f) = \sum |s(f)|$, with $S(f)$ represented as the total PSD spectrum of the system. We mainly focused on the magnetic properties of antiskyrmions, but for comparison, similar simulations on skyrmions were also performed. Two different methods were applied to excite the magnetic dynamics in skyrmions or antiskyrmions. As shown in Fig. 1(c), the uniform ac field $\widetilde{h}_z$ is applied on the whole structure, which can excite the breathing mode [53]. The ac field was also applied locally in a fan-shaped area with an azimuthal angle range of $10°$, as shown in Fig. 1(d). Then the locally excited magnetization dynamics can propagate azimuthally, which can further excite the azimuthal spin wave modes [54]. The strength of the excitation field $\mu_0 h_0$ is set as 0.5 mT for the uniform excitation in Fig. 1(c) and 10 mT for the nonuniform excitation in Fig. 1(d), respectively.

III. RESULTS AND DISCUSSION

A. Field-dependent evolution of an antiskyrmion

We first investigated the field-dependent evolution of an antiskyrmion at zero field; an antiskyrmion can only exist for 1.75 mJ m$^{-2} < D < 5.5$ mJ m^{-2}. For $D < 1.75$ mJ m^{-2}, only the single domain can be stabilized, and for $D > 5.5$ mJ m^{-2}, the lowest energy state is the stripe domain. The D-dependent evolution of an antiskyrmion is very similar to that of a skyrmion with the same parameters [53]. Figure 2(a) shows the typical spin configurations of antiskyrmions with different H_z for the systems with $D = 3$ mJ m^{-2} and $D = 4.5$ mJ m^{-2}, respectively. Due to Zeeman energy, the core of an antiskyrmion increases with positive H_z, and decreases with negative H_z. For a strong enough positive H_z, the core approaches the disk edge, and then the whole system will switch into a single domain with the switching field increasing with D. While expanding the core size with $+H_z$, the core shape gradually deforms from a circle shape into a square shape with the edge along the $\pm 45°$ directions. In this case, the length of the Bloch-type walls has a longer length than that of
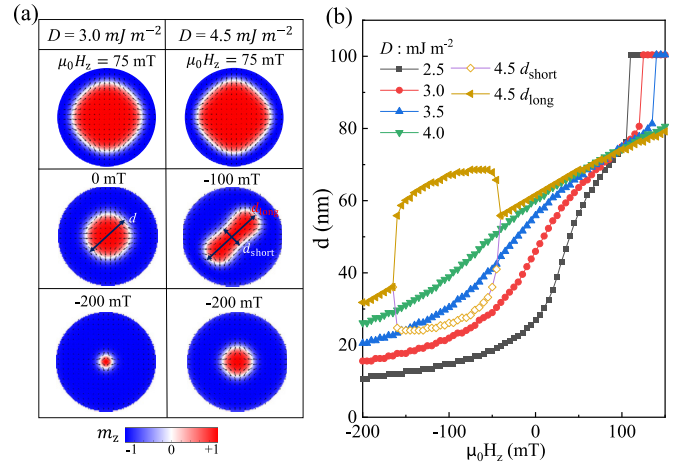

FIG. 2. (a) Representative magnetization distributions of antiskyrmions for $D = 3.0$ mJ m^{-2} and $D = 4.5$ mJ m^{-2} with different H_z. The diameter d of the circular antiskyrmion and the lengths d_{long} and d_{short} of the elongated antiskyrmion are defined by the black arrows. (b) The field-dependent evolution of the diameter d for the antiskyrmions with different D. For $D = 4.5$ mJ m^{-2}, the antiskyrmion is deformed into the elongated shape for a negative range of D, as shown in (a); thus d_{long} and d_{short} are plotted separately.

the Néel-type wall. This behavior is different from the field-dependent evolution of skyrmions, in which the core always shows a circular shape [50]. Note that the Bloch-type wall has a lower energy than the Néel-type wall; thus the system has the tendency to reduce the total energy by increasing the length of the Bloch-type wall [55]. However, in the system with $D = 4.5$ mJ m^{-2}, the circular core can be deformed into the elongated shape for $\mu_0 H_z$ between -55 and -155 mT. This elongation deformation is similar to that of a skyrmion reported in Ref. [53], where the field-dependent evolution of the skyrmion also contains an elongated distortion due to the competition between the Zeeman energy and DMI. For an antiskyrmion, the long axis of the elongated core stochastically aligns along the directions $45°$ or $-45°$ away from the $+x$ axis, making the Bloch-type wall longer than the Néel-type wall to reduce the dipole energy.

We conducted similar simulations in larger disks with diameters of 200 and 400 nm (see Supplemental Material [52]). In these cases, antiskyrmions with a circular core were stabilized within a smaller range of D, highlighting the significant role of geometric confinement in antiskyrmion stabilization.

B. Dynamic response of uniform excitation

Next, we studied the dynamic properties of the single antiskyrmion as a function of the static field ranging from -150 to $+150$ mT with a 5 mT step. The micromagnetic simulation was performed with $D = 3.0$ mJ m^{-2}. The antiskyrmion is initially relaxed to the equilibrium state under static field H_z, and then is further excited by the alternating $\widetilde{h}_z$. For comparison, we also studied the dynamic properties of the skyrmion with $D = 3.0$ mJ m^{-2} [53]. Figures 3(a) and 3(b) show the obtained PSD spectra at $\mu_0 H_z = 0$ and 75 mT for the skyrmion and antiskyrmion, respectively. Consistent with the studies in Ref. [53], there are three resonant modes
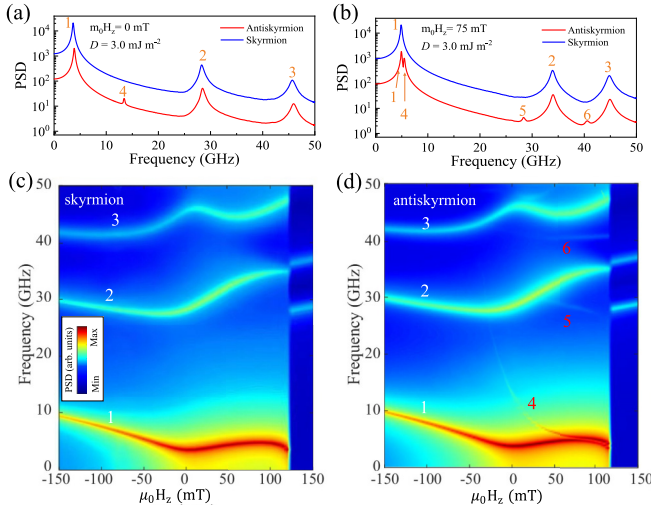
FIG. 3. Representative power spectral density (PSD) spectra at (a) $\mu_0 H_z = 0$ mT, and (b) $\mu_0 H_z = 75$ mT for a skyrmion and an antiskyrmion, respectively. (c,d) Color maps of PSD as a function of the static field H_z for (c) a skyrmion and (d) an antiskyrmion. The modes 1, 2, and 3 denote the excitations existing in both skyrmions and antiskyrmions, and the modes 4, 5, and 6 denote the unique excitations only existing in the antiskyrmion.
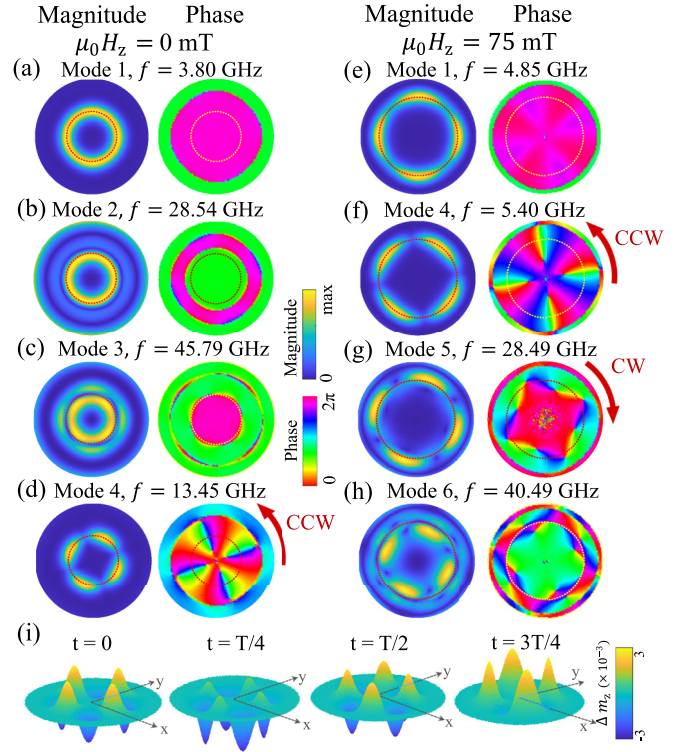

FIG. 4. Spatial profiles of the magnitude and phase of different modes on an antiskyrmion with corresponding eigenfrequencies at (a–d) $\mu_0 H_z = 0$ mT and (e–h) $\mu_0 H_z = 75$ mT. The dashed lines in the maps indicate locations of the domain wall. (i) Snapshots of temporal evolution of the magnetization within a single oscillation period for the spin wave mode 4 in (d) at $\mu_0 H_z = 0$ mT. The magnetization oscillation in the domain wall exhibits a clear counterclockwise rotation.

in the skyrmion, which also exist in the antiskyrmion with almost the same frequency. Furthermore, there is one additional excitation mode in the antiskyrmion at zero field, and three additional modes appear at $\mu_0 H_z = 75$ mT.

Figures 3(c) and 3(d) show the color maps of PSD for the skyrmion and antiskyrmion, respectively. Due to the transition into the uniform magnetization state at strong $+H_z$, the PSD maps of both skyrmion and antiskyrmion present an abrupt change at ~115 mT. The PSD of the skyrmion in Fig. 3(c) shows three excitation modes which are marked by the numbers 1, 2, and 3, respectively. These are the breathing modes of the core, fully agreeing with the previous study in Ref. [53], and the field-dependent evolution of those modes was attributed to the field-dependent change of the spin configuration. The same breathing modes also exist in the antiskyrmion. Additionally, three new modes can be identified for the antiskyrmion, as marked by the numbers 4, 5, and 6. Modes 5 and 6 only exist within a limited frequency range and for fields larger than 45 mT, but mode 4 could exist within a large frequency range for fields higher than −40 mT. For fields above 60 mT, mode 4 approaches mode 1, but they always repel each other, indicating the existence of coupling between these two dynamical modes.

In order to clarify the origin of the emerging dynamic modes in the antiskyrmion, we calculated the spatial profiles of each mode. The magnetization oscillation of each cell can be expressed as $\widetilde{m_z}(t) \sim m_z e^{-i(2\pi f t + \psi)}$; thus through the FFT analysis, the spatial distribution of magnitude m_z and the phase ψ of each dynamical mode at corresponding eigenfrequency can be obtained. Figures 4(a)–4(d) show the spatial distributions of magnitude and phase of four eigenmodes at $\mu_0 H_z = 0$ mT. It is clear that mode 1 with $f = 3.8$ GHz is the breathing mode with the magnetization oscillation happening locally around the core; thus the size of the antiskyrmion

core periodically changes under the oscillating field $\widetilde{h_z}$. Mode 2 at $f = 28.54$ GHz and mode 3 at $f = 45.79$ GHz correspond to the hybridization modes between the breathing mode and the radial spin wave mode. These three modes are almost the same as the modes in the skyrmion reported in Ref. [53].

As shown in Fig. 3, mode 4 is the additional mode in the antiskyrmion; thus in Fig. 4(d) we present the spatial profile of mode 4 with the eigenfrequency of 13.45 GHz at zero field. The magnetization oscillation also locates around the domain wall with four nodes. The phase of this mode shows the azimuthal change with a clockwise increase, so mode 4 is corresponds to an azimuthal spin wave propagating counterclockwise. The total phase change shown in Fig. 4(d) is 8π for the spin wave propagating by one round, so its wavelength is one-quarter of the domain wall circumference.

Figures 4(e)–4(h) present the lateral profiles of four representative modes in the antiskyrmion at $\mu_0 H_z = 75$ mT. Figure 4(e) shows mode 1 with $f = 4.85$ GHz, in which the magnitude shows four nodes, but the phase only has a slight variation, so this mode is also the breathing mode of the antiskyrmion. All three modes, 4–6, in Figs. 4(f)–4(h) show four nodes azimuthally with the phase change of 8π; thus all those modes should be related to the azimuthal spin wave modes. Note that the phase profiles in Figs. 4(g) and 4(h)
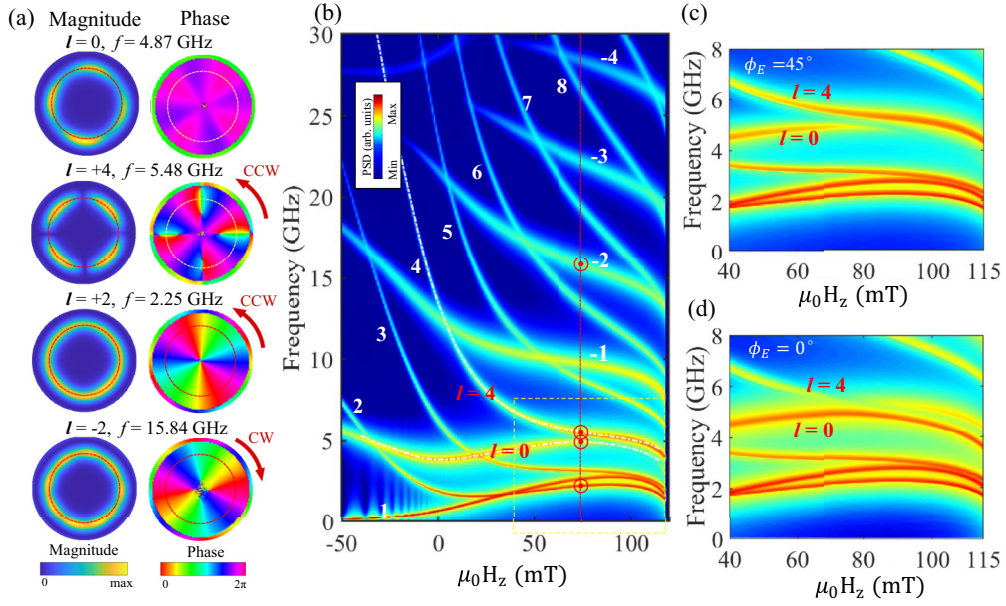
FIG. 5. (a) The representative spatial profile of dynamic modes on an antiskyrmion with different mode index l at $\mu_0 H_z = 75$ mT. (b) Map of PSD with spatially nonuniform ac field excitation at $\phi_E = 45°$. The white dashed curves in (b) indicate the frequency dispersion of the modes with $l = 0$ and $l = 4$ simulated for the uniform excitation. The red circles on the red dashed line correspond to four profiles in (a). (c) The enlarged PSD map indicated by the white dashed rectangle in (b). (d) The PSD map under nonuniform excitation at $\phi_E = 0°$.

show the complicated distribution without radial symmetry, indicating these two modes may be the hybridization mode between the azimuthal spin wave mode and the radial spin wave mode.

In order to better present the nature of the propagation around the core for the azimuthal spin wave mode, we also present the time-dependent evolutions of the azimuthal spin wave modes. Figure 4(i) shows the snapshots for the azimuthal spin wave mode with four nodes at different times during one oscillation period. The oscillations were excited by an ac field with a sinusoidal function, operating at the frequency of 13.45 GHz. Moreover, to showcase the time-dependent dynamics of the antiskyrmion in real space, we created supplemental videos for all the spin wave modes presented in Figs. 4 and 5, and presented them in the Supplemental Material [52].

Given that the additional modes in antiskyrmions arise from azimuthal spin waves, we further excite the azimuthal modes by applying the oscillating field $\tilde{h}_z$ only in a small angular range, as shown in Fig. 1(d). The field $\tilde{h}_z$ locally excites oscillations of the in-plane magnetization, which further excite spin waves propagating along the domain wall. If the phase change of the azimuthal spin waves is l times 2π, a resonant spin wave mode with the node number l can form [54]. The spin waves can propagate either clockwise or counterclockwise, which corresponds to the positive or negative index number l of the azimuthal spin wave mode. In thin films with the interfacial DMI, the spin waves propagating along two opposite directions perpendicular to the magnetization have different energy dispersions [56,57]. Thus, the spin waves propagating clockwise (CW) or counterclockwise (CCW) inside the domain walls are expected to have different dispersions due to the DMI [54], and the azimuthal spin wave

modes with CW or CCW propagation with the same value of $|l|$ should have different eigenfrequencies.

Figure 5 shows the simulation results with nonuniform excitation. Figure 5(a) shows the typical spatial profiles of magnitude and phase for several modes with different l at $\mu_0 H_z = 75$ mT. The positive index l indicates counterclockwise propagation, while the negative l indicates clockwise propagation [54]. The $l = 0$ mode is the breathing mode, as indicated by the radially uniform phase. Figure 5(b) shows the field-dependent evolution of the azimuthal spin wave modes. All these azimuthal spin wave modes are eigenmodes, so they simply cross each other while varying the field. However, the $l = 0$ mode and the $l = +4$ mode show a coupling effect for the applied field above 60 mT. We found the coupling effect is different for the nonuniform ac field applied at different φ_E. When exited at $\varphi_E = 45°$, the $l = 0$ mode in Fig. 5(c) is very weak for $\mu_0 H_z > 60$ mT, but for the excitation with $\varphi_E = 0°$, the $l = +4$ mode in Fig. 5(d) becomes weak at $\mu_0 H_z \sim 75$ mT.

C. Discussion on the origin of mode coupling

The results in Figs. 4 and 5 clearly indicate the existence of the coupling between the breathing mode and the fourfold azimuthal spin wave mode in antiskyrmions, which does not exist in skyrmions. Such difference can be attributed to the distinct spin configuration in the domain wall of skyrmions and antiskyrmions, since skyrmions show rotational symmetry, while antiskyrmions only have azimuthal twofold symmetry. Figure 6 shows the lateral dipolar field distributions for both skyrmions and antiskyrmions. In a skyrmion, the total effective field B_{eff}, including the dipolar field and the exchange field, is independent of the azimuthal angle [Fig. 6(c)]. However, in an antiskyrmion, although its domain
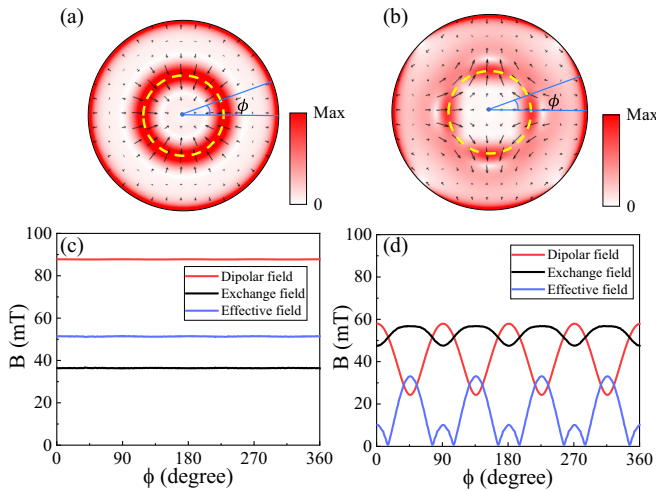
FIG. 6. In-plane components of dipolar fields for (a) a skyrmion and (b) an antiskyrmion at $\mu_0 H_z = 0$ mT with $D = 3.0$ mJ m^{-2}. The black arrows indicate the direction of local in-plane magnetization, and the yellow dashed line indicates the location of the domain wall. At the equilibrium state, the black arrows inside the domain walls also indicate the direction of total effective field B_{eff}. (c,d) The ϕ dependences of dipolar field, exchange field, and total effective field B_{eff} inside the domain walls of (c) a skyrmion and (d) an antiskyrmion, respectively.

wall still shows a circular shape, the effective field exhibits a clear fourfold symmetry as a function of azimuthal angle ϕ, with maxima at the Bloch-type wall positions ($\phi = 45°$, $135°$, $225°$, and $135°$), which is attributed to the difference of dipolar fields in the Bloch-type wall and the Néel-type wall [Fig. 6(d)].

Based on the analysis of the rotation-symmetry breaking in antiskyrmions, the excitation of the fourfold azimuthal spin wave mode under uniform field excitation can be further understood. Under the excitation of the uniform $\tilde{h}_z(t)$, the oscillation of magnetization mostly locates around the domain wall with the in-plane magnetization component, and should be roughly inversely proportional to the local in-plane effective field strength B_{eff}, i.e., $\tilde{m}_z(t) \propto \frac{\tilde{h}_z(t)}{B_{\text{eff}}}$. The excited magnetization dynamics will further excite the spin wave propagating along the domain wall. The different effective fields at the Bloch-type wall and the Néel-type wall result in the different magnetization excitations at different locations. Due to the fourfold effective field, the azimuthal spin waves with a wavelength equal to one-quarter of the circumference of the domain wall will be resonantly excited to form a standing wave, which is the observed azimuthal spin wave mode in Fig. 4. Based on this analysis, only the fourfold azimuthal spin wave mode can be excited under the uniform ac field in antiskyrmions. In principle, the spin wave mode with $l = -4$ could be excited as well under the uniform ac field. However, Fig. 5 shows that the frequency of the $l = -4$ mode is much higher than that of the breathing mode, so such spin wave mode could be too weak to be observed. In fact, mode 5 at $\mu_0 H_z = 75$ mT shown in Fig. 4(g) can be considered as the $l = -4$ spin wave mode, and this mode is also coupled with the radial spin wave mode; thus its azimuthal phase change

shows a complicated angular dependence in comparison with the $l = +4$ spin wave mode in Fig. 4(f).

The coupling between the breathing mode and the fourfold azimuthal spin wave in antiskyrmions can be understood in the following way. In the breathing mode, the magnetization oscillation at the domain wall can also induce the spin wave propagation, and excite the resonant azimuthal spin wave with $l = +4$ or $l = -4$, resulting in mode coupling between the breathing mode and the azimuthal spin wave mode. As shown in Fig. 5(b), the $l = +4$ azimuthal spin wave mode has a frequency close to the breathing mode for $\mu_0 H_z > 60$ mT; thus the mode coupling could be stronger under this condition.

In a skyrmion or an antiskyrmion, all the excited magnetic dynamics can be regarded as a local source of spin wave emission. However, compared to the antiskyrmion, a skyrmion has rotational symmetry, and all the excited azimuthal spin waves are fully canceled. This is the reason that no azimuthal spin wave can be observed [53]. In this case, if the rotational symmetry in a skyrmion is broken, azimuthal spin wave modes can also be excited by the uniform ac field. Indeed, in the elliptical skyrmions with shape deformation, such an azimuthal spin wave was observed in the micromagnetic simulations [58]. However, without changing the skyrmion shape, the azimuthal spin wave can be excited by breaking the rotational symmetry of the spin configuration in the domain wall. Here, we first applied an in-plane fourfold anisotropy to the skyrmion system, which may exist in the crystalline CoFeB films grown on MgO(001) [17,59,60]. The in-plane fourfold anisotropy energy density can be expressed as $\varepsilon_4 = -K_4 m_x^2 m_y^2$; thus the in-plane easy axis is $45°$ away from the x axis. In the simulation, we applied the anisotropy energy as $K_4 = 5 \times 10^4$ J m^{-3}, and calculated the magnetization excitation at zero field under the uniform ac field. As shown in Fig. 7(a), such a small anisotropy will not induce an observable shape change of the skyrmion core but can induce a fourfold symmetry of the effective field B_{eff}. Indeed, an additional mode can be observed, as indicated by the red arrow in Fig. 7(a). The spatial profiles of magnitude and phase in Fig. 7(b) confirm that this mode is the azimuthal spin wave mode with $l = -4$. Our calculation shows that such a new mode could be excited by a fourfold anisotropy as low as 2.5×10^4 J m^{-3}.

Similarly, a twofold azimuthal spin wave mode can be excited if a small in-plane twofold anisotropy is applied [Fig. 7(c)]. We set the in-plane twofold anisotropy energy as $\varepsilon_2 = -K_2 m_u^2$, where K_2 is the in-plane uniaxial anisotropy constant and m_u is the magnetization projection along the in-plane easy axis. In this calculation, the in-plane easy axis was set at a $45°$ angle away from the x axis. This new mode can be excited in the skyrmion system with $K_2 = 8 \times 10^3$ J m^{-3}, and the spatial profiles of magnitude and phase in Fig. 7(d) confirm that this is the azimuthal spin wave mode with $l = -2$. Although the skyrmion shows a clear circular shape, such a small uniaxial anisotropy can still induce a strong variation of B_{eff} inside the domain wall. In this way, we have demonstrated that the introduction of n-fold symmetry breaking in B_{eff} inside the domain wall enables the induction of azimuthal spin waves with an index of n through uniform field excitation. While earlier investigations have demonstrated that the shape deformation of skyrmions can induce mode coupling
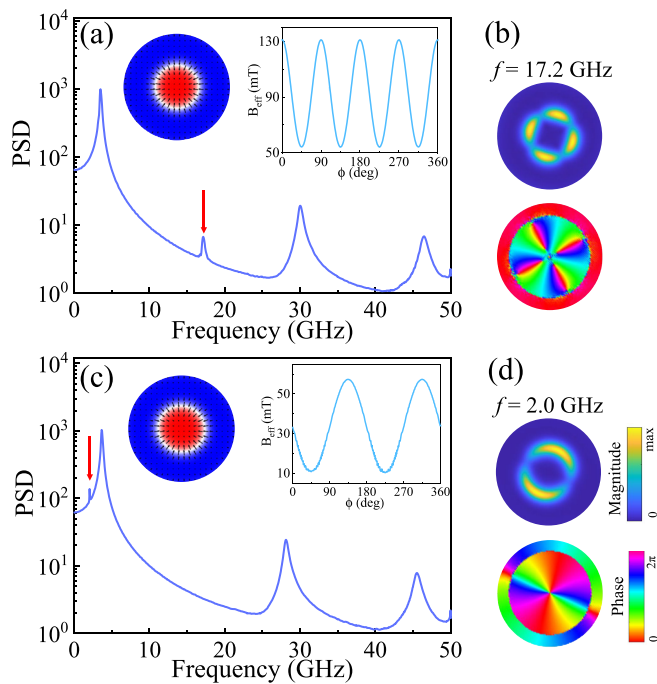
FIG. 7. (a) PSD under uniform excitation in a skyrmion with a small in-plane fourfold anisotropy of $K_4 = 5 \times 10^4$ J m^{-3}. The insets show the magnetization distribution of the skyrmion and the ϕ-dependent effective field strength B_{eff} inside the domain wall. (b) The spatial profiles of magnitude and phase for the additional mode in (a) marked by the red arrow. (c) PSD under uniform excitation in a skyrmion with a small in-plane twofold anisotropy of $K_2 = 8 \times 10^3$ J m^{-3}; the insets show the magnetization distribution of the skyrmions and the ϕ-dependent effective field strength B_{eff}. (d) The spatial profiles of magnitude and phase for the additional mode in (c) marked by the red arrow.

between the breathing mode and the azimuthal spin wave mode [61,62], our results emphasize that such deformation is not mandatory. Even a subtle symmetry breaking in the spin configuration can adeptly manipulate mode coupling in this topological spin system. In addition to antiskyrmions, other topological spin structures, such as bimerons [63,64], also exhibit broken rotational symmetry. Consequently, mode coupling between the breathing mode and azimuthal

spin wave mode should also be present in such spin structures.

IV. SUMMARY

In summary, we have studied the field-dependent evolution of antiskyrmions and their microwave field excited magnetic dynamics, including breathing modes and azimuthal spin wave modes. Due to the lower dipolar energy, Bloch-type rotations are favored over Néel-type rotations, leading to the formation of an antiskyrmion core with a square or elongated shape. Under uniform microwave excitation, antiskyrmions not only present the same breathing modes in skyrmions, but also show fourfold azimuthal spin wave modes. Excitation by localized ac magnetic field also demonstrates such mode coupling between the breathing mode and the fourfold azimuthal spin wave mode. This unusual coupling arises from the intrinsic spin configuration due to the rotational symmetry breaking in antiskyrmions. We further showed that in a skyrmion with rotational symmetric shape, such a mode coupling between the breathing mode and the azimuthal spin wave mode can also exist with a small in-plane magnetic anisotropy. Such mode coupling can be investigated potentially in antiskyrmion systems [33,34] or skyrmion systems [1–3] with varying magnetic anisotropy, tuned by strain. Our study on the magnetic dynamics of antiskyrmions provides further insights into the topological chiral textures. Furthermore, detecting these resonant oscillation modes experimentally may offer a way to characterize the states of skyrmions and antiskyrmions in confined structures, opening up opportunities for designing spintronic devices.

[1] X. Z. Yu, Y. Onose, N. Kanazawa, J. H. Park, J. H. Han, Y. Matsui, N. Nagaosa, and Y. Tokura, Real-space observation of a two-dimensional Skyrmion crystal, Nature (London) **465**, 901 (2010).

[2] S. Heinze, K. von Bergmann, M. Menzel, J. Brede, A. Kubetzka, R. Wiesendanger, G. Bihlmayer, and S. Blugel, Spontaneous atomic-scale magnetic skyrmion lattice in two dimensions, Nat. Phys. **7**, 713 (2011).

[3] O. Boulle, J. Vogel, H. X. Yang, S. Pizzini, D. D. Chaves, A. Locatelli, T. O. Mentes, A. Sala, L. D. Buda-Prejbeanu, O. Klein, M. Belmeguenai, Y. Roussigne, A. Stashkevich, S. M. Cherif, L. Aballe, M. Foerster, M. Chshiev, S. Auffret, I. M. Miron, and G. Gaudin, Room-temperature chiral magnetic skyrmions in ultrathin magnetic nanostructures, Nat. Nanotechnol. **11**, 449 (2016).

[4] A. Fert, N. Reyren, and V. Cros, Magnetic skyrmions: Advances in physics and potential applications, Nat. Rev. Mater. **2**, 17031 (2017).

[5] W. J. Jiang, G. Chen, K. Liu, J. D. Zang, S. G. E. te Velthuis, and A. Hoffmann, Skyrmions in magnetic multilayers, Phys. Rep. **704**, 1 (2017).

[6] G. Finocchio, F. Buttner, R. Tomasello, M. Carpentieri, and M. Klaui, Magnetic skyrmions: From fundamental to applications, J. Phys. D **49**, 423001 (2016).

[7] T. Moriya, Anisotropic superexchange interaction and weak ferromagnetism, Phys. Rev. **120**, 91 (1960).

[8] A. N. Bogdanov and U. K. Rossler, Chiral symmetry breaking in magnetic thin films and multilayers, Phys. Rev. Lett. **87**, 037203 (2001).

[9] S. A. Montoya, S. Couture, J. J. Chess, J. C. T. Lee, N. Kent, D. Henze, S. K. Sinha, M. Y. Im, S. D. Kevan, P. Fischer, B. J. McMorran, V. Lomakin, S. Roy, and E. E. Fullerton, Tailoring magnetic energies to form dipole skyrmions and skyrmion lattices, Phys. Rev. B **95**, 024415 (2017).

[10] S. A. Montoya, S. Couture, J. J. Chess, J. C. T. Lee, N. Kent, M. Y. Im, S. D. Kevan, P. Fischer, B. J. McMorran, S. Roy, V. Lomakin, and E. E. Fullerton, Resonant properties of dipole skyrmions in amorphous Fe/Gd multilayers, Phys. Rev. B **95**, 224405 (2017).

[11] M. Heigl, S. Koraltan, M. Vanatka, R. Kraft, C. Abert, C. Vogler, A. Semisalova, P. Che, A. Ullrich, T. Schmidt, J. Hintermayr, D. Grundler, M. Farle, M. Urbánek, D. Suess, and M. Albrecht, Dipolar-stabilized first and second-order antiskyrmions in ferrimagnetic multilayers, Nat. Commun. **12**, 2611 (2021).

[12] S.-Z. Lin and S. Hayami, Ginzburg-Landau theory for skyrmions in inversion-symmetric magnets with competing interactions, Phys. Rev. B **93**, 064430 (2016).

[13] X. Zhang, J. Xia, Y. Zhou, X. Liu, H. Zhang, and M. Ezawa, Skyrmion dynamics in a frustrated ferromagnetic film and current-induced helicity locking-unlocking transition, Nat. Commun. **8**, 1717 (2017).

[14] S. Hayami, Multifarious skyrmion phases on a trilayer triangular lattice, Phys. Rev. B **105**, 184426 (2022).

[15] S. Mühlbauer, B. Binz, F. Jonietz, C. Pfleiderer, A. Rosch, A. Neubauer, R. Georgii, and P. Böni, Skyrmion lattice in a chiral magnet, Science **323**, 915 (2009).

[16] G. Chen, A. Mascaraque, A. T. N'Diaye, and A. K. Schmid, Room temperature skyrmion ground state stabilized through interlayer exchange coupling, Appl. Phys. Lett. **106**, 242404 (2015).

[17] W. J. Jiang, P. Upadhyaya, W. Zhang, G. Q. Yu, M. B. Jungfleisch, F. Y. Fradin, J. E. Pearson, Y. Tserkovnyak, K. L. Wang, O. Heinonen, S. G. E. te Velthuis, and A. Hoffmann, Blowing magnetic skyrmion bubbles, Science **349**, 283 (2015).

[18] S. D. Pollard, J. A. Garlow, J. W. Yu, Z. Wang, Y. M. Zhu, and H. Yang, Observation of stable Néel skyrmions in cobalt/palladium multilayers with Lorentz transmission electron microscopy, Nat. Commun. **8**, 14761 (2017).

[19] G. Chen, J. Zhu, A. Quesada, J. Li, A. T. N'Diaye, Y. Huo, T. P. Ma, Y. Chen, H. Y. Kwon, C. Won, Z. Q. Qiu, A. K. Schmid, and Y. Z. Wu, Novel chiral magnetic domain wall structure in Fe/Ni/Cu(001) films, Phys. Rev. Lett. **110**, 177204 (2013).

[20] A. Fert, V. Cros, and J. Sampaio, Skyrmions on the track, Nat. Nanotechnol. **8**, 152 (2013).

[21] R. Tomasello, E. Martinez, R. Zivieri, L. Torres, M. Carpentieri, and G. Finocchio, A strategy for the design of skyrmion racetrack memories, Sci. Rep. **4**, 6784 (2014).

[22] R. H. Liu, W. L. Lim, and S. Urazhdin, Dynamical skyrmion state in a spin current nano-oscillator with perpendicular magnetic anisotropy, Phys. Rev. Lett. **114**, 137201 (2015).

[23] G. Finocchio, M. Ricci, R. Tomasello, A. Giordano, M. Lanuzza, V. Puliafito, P. Burrascano, B. Azzerboni, and M. Carpentieri, Skyrmion based microwave detectors and harvesting, Appl. Phys. Lett. **107**, 262401 (2015).

[24] K. M. Song, J. S. Jeong, B. Pan, X. C. Zhang, J. Xia, S. Cha, T. E. Park, K. Kim, S. Finizio, J. Raabe, J. Chang, Y. Zhou, W. S. Zhao, W. Kang, H. S. Ju, and S. Woo, Skyrmion-based artificial synapses for neuromorphic computing, Nat. Electron. **3**, 148 (2020).

[25] D. Prychynenko, M. Sitte, K. Litzius, B. Kruger, G. Bourianoff, M. Klaui, J. Sinova, and K. Everschor-Sitte, Magnetic skyrmion as a nonlinear resistive element: A potential building block for reservoir computing, Phys. Rev. Appl. **9**, 014034 (2018).

[26] X. C. Zhang, Y. Zhou, K. M. Song, T. E. Park, J. Xia, M. Ezawa, X. X. Liu, W. S. Zhao, G. P. Zhao, and S. Woo, Skyrmion-electronics: Writing, deleting, reading and processing magnetic skyrmions toward spintronic applications, J. Phys.: Condens. Matter **32**, 143001 (2020).

[27] A. A. Kovalev and S. Sandhoefner, Skyrmions and antiskyrmions in quasi-two-dimensional magnets, Front. Phys. **6**, 98 (2018).

[28] W. Koshibae and N. Nagaosa, Theory of antiskyrmions in magnets, Nat. Commun. **7**, 10542 (2016).

[29] M. Hoffmann, B. Zimmermann, G. P. Muller, D. Schurhoff, N. S. Kiselev, C. Melcher, and S. Blugel, Antiskyrmions stabilized at interfaces by anisotropic Dzyaloshinskii-Moriya interactions, Nat. Commun. **8**, 308 (2017).

[30] L. Camosi, N. Rougemaille, O. Fruchart, J. Vogel, and S. Rohart, Micromagnetics of antiskyrmions in ultrathin films, Phys. Rev. B **97**, 134404 (2018).

[31] N. Nagaosa and Y. Tokura, Topological properties and dynamics of magnetic skyrmions, Nat. Nanotechnol. **8**, 899 (2013).

[32] S. Huang, C. Zhou, G. Chen, H. Shen, A. K. Schmid, K. Liu, and Y. Wu, Stabilization and current-induced motion of antiskyrmion in the presence of anisotropic Dzyaloshinskii-Moriya interaction, Phys. Rev. B **96**, 144412 (2017).

[33] A. K. Nayak, V. Kumar, T. P. Ma, P. Werner, E. Pippel, R. Sahoo, F. Damay, U. K. Rossler, C. Felser, and S. S. P. Parkin, Magnetic antiskyrmions above room temperature in tetragonal Heusler materials, Nature (London) **548**, 561 (2017).

[34] J. Jena, R. Stinshoff, R. Saha, A. K. Srivastava, T. P. Ma, H. Deniz, P. Werner, C. Felser, and S. S. P. Parkin, Observation of magnetic antiskyrmions in the low magnetization ferrimagnet $Mn_2Rh_{0.95}Ir_{0.05}Sn$, Nano Lett. **20**, 59 (2020).

[35] M. Mochizuki, Spin-wave modes and their intense excitation effects in skyrmion crystals, Phys. Rev. Lett. **108**, 017601 (2012).

[36] Y. Onose, Y. Okamura, S. Seki, S. Ishiwata, and Y. Tokura, Observation of magnetic excitations of skyrmion crystal in a helimagnetic insulator Cu_2OSeO_3, Phys. Rev. Lett. **109**, 037603 (2012).

[37] S. A. Díaz, T. Hirosawa, D. Loss, and C. Psaroudaki, Spin wave radiation by a topological charge dipole, Nano Lett. **20**, 6556 (2020).

[38] J. L. Chen, J. F. Hu, and H. M. Yu, Chiral emission of exchange spin waves by magnetic skyrmions, ACS Nano **15**, 4372 (2021).

[39] S. Pollath, A. Aqeel, A. Bauer, C. Luo, H. Ryll, F. Radu, C. Pfleiderer, G. Woltersdorf, and C. H. Back, Ferromagnetic resonance with magnetic phase selectivity by means of resonant elastic x-ray scattering on a chiral magnet, Phys. Rev. Lett. **123**, 167201 (2019).

[40] A. Aqeel, J. Sahliger, T. Taniguchi, S. Mandl, D. Mettus, H. Berger, A. Bauer, M. Garst, C. Pfleiderer, and C. H. Back, Microwave spectroscopy of the low-temperature skyrmion state in Cu_2OSeO_3, Phys. Rev. Lett. **126**, 017202 (2021).

[41] D. M. Burn, S. L. Zhang, G. van der Laan, and T. Hesjedal, Time-resolved measurement of spin excitations in Cu_2OSeO_3, Phys. Rev. B **106**, 174409 (2022).

[42] Y. Okamura, F. Kagawa, M. Mochizuki, M. Kubota, S. Seki, S. Ishiwata, M. Kawasaki, Y. Onose, and Y. Tokura, Microwave magnetoelectric effect via skyrmion resonance modes in a helimagnetic multiferroic, Nat. Commun. **4**, 2391 (2013).

[43] B. Satywali, V. P. Kravchuk, L. Pan, M. Raju, S. He, F. Ma, A. P. Petrović, M. Garst, and C. Panagopoulos, Microwave resonances of magnetic skyrmions in thin film multilayers, Nat. Commun. **12**, 1909 (2021).

[44] O. S. Lee, J. Sahliger, A. Aqeel, S. Khan, S. Seki, H. Kurebayashi, and C. H. Back, Tunable gigahertz dynamics of low-temperature skyrmion lattice in a chiral magnet, J. Phys.: Condens. Matter **34**, 095801 (2022).

[45] R. Takagi, M. Garst, J. Sahliger, C. H. Back, Y. Tokura, and S. Seki, Hybridized magnon modes in the quenched skyrmion crystal, Phys. Rev. B **104**, 144410 (2021).

[46] X. J. Liu, L. Q. Guo, H. Wang, and Z. K. Tang, The internal dynamic modes of an antiskyrmion in ultrathin ferromagnetic nanodisks, AIP Adv. **10**, 075222 (2020).

[47] C. K. Song, C. D. Jin, Y. X. Ma, J. S. Wang, H. Y. Xia, J. B. Wang, and Q. F. Liu, Trochoidal antiskyrmion motion with microwave electric fields, J. Phys. D **52**, 435001 (2019).

[48] A. Vansteenkiste, J. Leliaert, M. Dvornik, M. Helsen, F. Garcia-Sanchez, and B. Van Waeyenberge, The design and verification of MuMax3, AIP Adv. **4**, 107133 (2014).

[49] T. L. Gilbert, A phenomenological theory of damping in ferromagnetic materials, IEEE Trans. Magn. **40**, 3443 (2004).

[50] J. Sampaio, V. Cros, S. Rohart, A. Thiaville, and A. Fert, Nucleation, stability and current-induced motion of isolated magnetic skyrmions in nanostructures, Nat. Nanotechnol. **8**, 839 (2013).

[51] F. Garcia-Sanchez, P. Borys, A. Vansteenkiste, J. V. Kim, and R. L. Stamps, Nonreciprocal spin-wave channeling along textures driven by the Dzyaloshinskii-Moriya interaction, Phys. Rev. B **89**, 224408 (2014).

[52] See Supplemental Material at http://link.aps.org/supplemental/10.1103/PhysRevB.109.104431 for the micromagnetic simulations on the square disk and the circular disk with different diameters and the summary of the movies for the spin wave modes shown in this paper.

[53] J. V. Kim, F. Garcia-Sanchez, J. Sampaio, C. Moreau-Luchaire, V. Cros, and A. Fert, Breathing modes of confined skyrmions in ultrathin magnetic dots, Phys. Rev. B **90**, 064410 (2014).

[54] M. Mruczkiewicz, P. Gruszecki, M. Krawczyk, and K. Y. Guslienko, Azimuthal spin-wave excitations in magnetic nanodots over the soliton background: Vortex, Bloch, and Néel-like skyrmions, Phys. Rev. B **97**, 064418 (2018).

[55] G. Chen, T. P. Ma, A. T. N'Diaye, H. Kwon, C. Won, Y. Z. Wu, and A. K. Schmid, Tailoring the chirality of magnetic domain walls by interface engineering, Nat. Commun. **4**, 2671 (2013).

[56] K. Di, V. L. Zhang, H. S. Lim, S. C. Ng, M. H. Kuok, J. Yu, J. Yoon, X. Qiu, and H. Yang, Direct observation of the Dzyaloshinskii-Moriya interaction in a Pt/Co/Ni film, Phys. Rev. Lett. **114**, 047201 (2015).

[57] J.-H. Moon, S.-M. Seo, K.-J. Lee, K.-W. Kim, J. Ryu, H.-W. Lee, R. D. McMichael, and M. D. Stiles, Spin-wave propagation in the presence of interfacial Dzyaloshinskii-Moriya interaction, Phys. Rev. B **88**, 184404 (2013).

[58] Y. Z. Liu, R. K. Lake, and J. D. Zang, Shape dependent resonant modes of skyrmions in magnetic nanodisks, J. Magn. Magn. Mater. **455**, 9 (2018).

[59] A. K. Kaveev, V. E. Bursian, B. B. Krichevtsov, K. V. Mashkov, S. M. Suturin, M. P. Volkov, M. Tabuchi, and N. S. Sokolov, Laser MBE-grown CoFeB epitaxial layers on MgO: Surface morphology, crystal structure, and magnetic properties, Phys. Rev. Mater. **2**, 014411 (2018).

[60] Z. G. Qin, C. D. Jin, H. K. Xie, X. L. Li, Y. Wang, J. W. Cao, and Q. F. Liu, Size-tunable skyrmion bubbles in Ta/CoFeB/MgO multilayers, J. Phys. D **51**, 425001 (2018).

[61] N. Mehmood, J. Wang, C. Zhang, Z. Zeng, J. Wang, and Q. Liu, Magnetic skyrmion shape manipulation by perpendicular magnetic anisotropy excitation within geometrically confined nanostructures, J. Magn. Magn. Mater. **545**, 168775 (2022).

[62] C. D. Jin, S. Li, H. Zhang, R. N. Wang, J. L. Wang, R. Q. Lian, P. L. Gong, and X. Q. Shi, Spin-wave modes of elliptical skyrmions in magnetic nanodots, New J. Phys. **24**, 043005 (2022).

[63] L. Shen, X. Li, J. Xia, L. Qiu, X. Zhang, O. A. Tretiakov, M. Ezawa, and Y. Zhou, Dynamics of ferromagnetic bimerons driven by spin currents and magnetic fields, Phys. Rev. B **102**, 104427 (2020).

[64] C. D. Jin, S. Li, H. Zhang, R. N. Wang, J. L. Wang, R. Q. Lian, P. L. Gong, and X. Q. Shi, Spin-wave modes of magnetic bimerons in nanodots, New J. Phys. **24**, 073013 (2022).